Arch. Mech., **51**, 6, pp. 833–845, Warszawa 1999

# Fatigue properties of TiNi shape memory alloy and applications to a heat engine and an actuator

H. TOBUSHI ([1]), T. NAKAHARA ([1]), T. HASHIMOTO ([1]), Y. SHIMENO ([1]) and K. TANAKA ([2])

([1]) *Department of Mechanical Engineering*
*Aichi Institute of Technology*
*1247 Yachigusa, Yagusa-cho, Toyota, 470–0392, Japan*
*E-mail: tobushi@me.aitech.ac.jp*

([2]) *Department of Aerospace Engineering*
*Tokyo Metropolitan Institute of Technology*
*Asahigaoka 6-6, Hino, Tokyo, 191–0065, Japan*

THE FATIGUE PROPERTIES of a TiNi shape-memory alloy (SMA) wire in the region of the martensitic transformation and the R-phase transformation are investigated. The rotating-bending fatigue life of a wire in the region of the R-phase transformation is longer than $10^7$ cycles. A tilt-disk offset SMA heat engine and an indirect-heated SMA thermal actuator are developed.

## 1. Introduction

THE SHAPE MEMORY EFFECT (SME) and the superelasticity (SE) appear in a shape memory alloy (SMA) [1, 2]. Using these properties, a SMA performs the two functions of a temperature sensor and a generator of working force. Furthermore, because the densities of dissipation and storage of strain energy are large, we can produce high performance elements. Thus applications of a SMA as smart materials have attracted interest. In applications to an actuator, a robot and a solid-state heat engine, a SMA is used as a working element that performs cyclic motions. Therefore, in order to evaluate the reliability of the SMA element, cyclic deformation properties of the material are important. In most SMAs, the SME and the SE appear as the result of monoclinic martensitic transformation (MT). In TiNi SMA, the SME and the SE appear also due to the rhombohedral-phase transformation (RPT) [3, 4]. In the RPT compared with the MT, strain is small but cyclic deformation properties are superior [5, 6]. In the SMA elements subjected to high-cycle deformation in a robot and a solid-state

heat engine, the fatigue life is also an important problem [7, 8]. From a viewpoint of heat transfer, thin wires are widely used as the SMA elements. Therefore, in order to evaluate the reliability of SMA elements, the fatigue properties of wires are necessary. If we use the SMA heat engines, low-grade thermal energy can be used [9, 10]. The SMA heat engines make no waste gas. From the viewpoint of energy crisis, the development of the SMA engines is expected. In the case of applications of SMA elements to vehicles, electric source is limited. If we use the SME or recovery force of SMA elements, the SMA elements are heated. In order to control movement of the SMA elements, low-level electric current is required. Therefore a new method to heat the SMA elements is necessary. In this work, the rotating-bending fatigue properties of a TiNi SMA wire in air and in water are investigated. The formulation of low cycle fatigue is investigated. A tilt-disk offset SMA heat engine and an indirect-heated SMA thermal actuator are developed.

## 2. Material and specimen

The material was a Ti-55.3wt%Ni SMA wire, 0.75 mm in diameter. The specimens were given shape memory of a straight line and a coiled spring through shape memory processing. The reverse-transformation completion temperature $A_f$ was about 323 K. The wires of a straight line were used for the rotating-bending fatigue tests. The coiled springs were used for a tilt-disk offset SMA heat engine and an indirect-heated SMA thermal actuator.

## 3. Rotating-bending fatigue

### 3.1 Experimental method

The rotating-bending fatigue test machines in air and in water were used [11]. In the tests, keeping the bent form of a SMA wire constant, the wire was rotated. The maximum strain on the surface of the wire was determined by the radius of bent curvature. The strain amplitude was the maximum strain in the middle of the wire between two supports. The temperature on the surface of the wire in air was measured through a thermograph.

The rotating-bending fatigue tests under constant strain amplitude $\varepsilon_a$, temperature $T$ and frequency $f$ were carried out in air and in water, and the number of cycles to failure was measured. The tests were performed for various values of $\varepsilon_a$, $T$ and $f$.

### 3.2. Fatigue in water and in air

The relationship between strain amplitude $\varepsilon_a$ and the number of cycles to failure $N_f$ obtained by the rotating-bending fatigue test at various test temperatures $T$ on a constant frequency $f = 500$ cpm in water is shown in Fig. 1. In Fig. 1, experimental data are plotted by several symbols and are connected by solid lines. As seen in Fig. 1, $N_f$ decreases with increasing both $\varepsilon_a$ and $T$. In the region of small $\varepsilon_a$, the strain-life relationship has the knee and approaches the horizontal line. The fatigue limit is in the region of $\varepsilon_a$ of $0.4 \sim 0.8\%$ depending on $T$. The inelastic part of strain $\varepsilon_a$ in this region is connected with RPT [3, 4]. Therefore the fatigue life is very long in the region of the RPT. Compared with the MT, the RPT strain is small and the fatigue damage due to the RPT is small, resulting in long fatigue life.

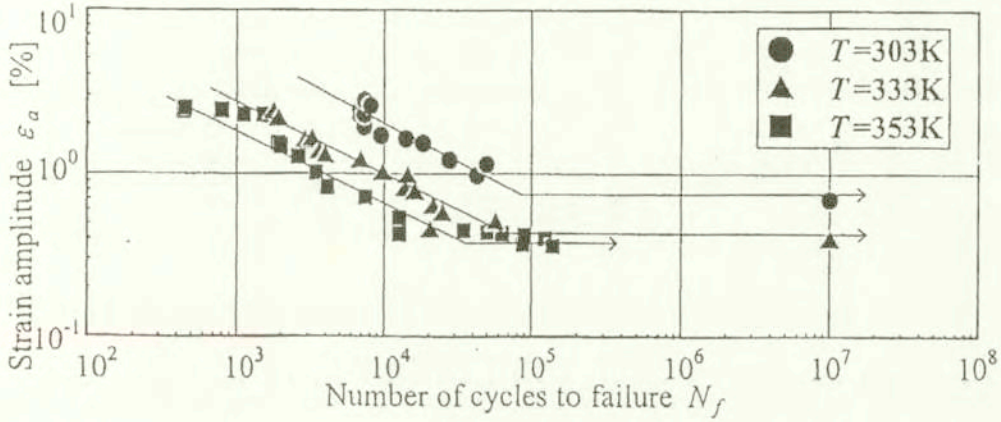


FIG. 1. Relationship between strain amplitude and number of cycles to failure at various temperatures in water on $f = 500$ cpm.

On the contrary, in the region of low-cycle fatigue for the MT strain $\varepsilon_a$ above 1%, the strain-life relationship is expressed by the straight line having a steep slope. The slopes of the lines at various temperatures are 0.5.

The relationship between the MT stress $\sigma_M$ and temperature $T$ may be expressed by the following equation called the transformation line [12]:

$$\sigma_M = C_M(T - M_s), \tag{3.1}$$

where $C_M$ and $M_s$ denote a slope of the transformation line and the MT starting temperature under no stress, respectively. As found from Eq. (3.1), $\sigma_M$ increases in proportion to $T$. Because $C_M$ is 6 MPa/K [13], $\sigma_M$ increases by 120 MPa if $T$ increases by 20 K. Thus, if temperature is high, the MT stress increases and fatigue damage is large, resulting in short fatigue life.

The relationships between strain amplitude $\varepsilon_a$ and the number of cycles to failure $N_f$ for two temperatures obtained by the rotating-bending fatigue test in air and in water performed at constant frequency $f = 500$ cpm are shown in Fig. 2. In the case marked with an arrow, the specimen did not rupture.

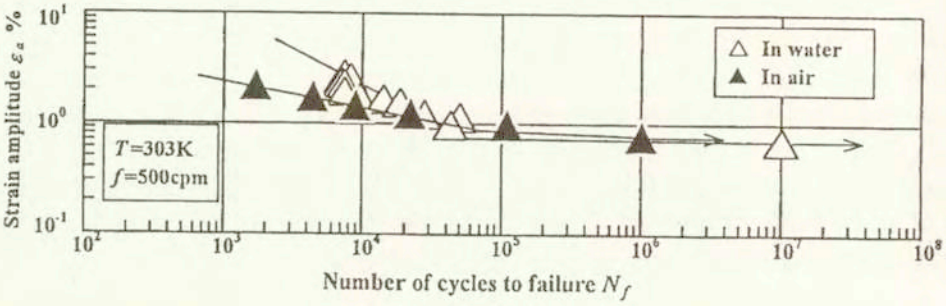


(a) $T$=303K

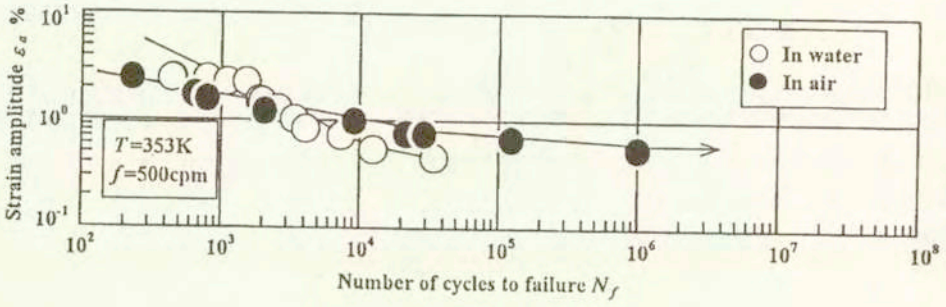


(b) T=353K

FIG. 2. Strain-life curves in air and in water on $f = 500$ cpm.

As seen in Fig. 2, the strain-life curves may be expressed by bi-linear lines. The strain-life curve has a knee in the region of $\varepsilon_a = 0.5 \sim 1\%$ and $N_f = 10^4 \sim 10^5$ cycles. In the region of $\varepsilon_a$ larger than the knee, the slope of the lines is large. On the contrary, in the region of $\varepsilon_a$ smaller than the knee, $N_f$ increases markedly and the lines approach the horizontal lines. These properties are similar as those observed in Fig. 1.

The region of $\varepsilon_a$ larger than the knee of strain-life curves is in the region after completion of the RPT and in the region of the MT. Let us discuss the slope of the lines in this region. Although the slopes of the lines are different in air and in water, both take almost the same values for each temperature. The value of slope is 0.24 in air but 0.5 in water. The value of 0.5 in water is almost the same as that for steel. The reason why the value of the slope is different for tests performed in air and in water can be explained as follows.

If $\varepsilon_a$ is large, dissipated work during the loading and unloading processes is large, resulting in large temperature rise $\Delta T$ under cyclic deformation in air. From Eq. (3.1), it is found that if temperature increases by $\Delta T = 10$ K, $\sigma_M$ increases by $\Delta\sigma_M = 60$ MPa. If stress on the surface of the wire increases, nucleation and growth of fatigue cracks are activated, resulting in small $N_f$. In air, if $\varepsilon_a$ is large, $\Delta T$ is large and $N_f$ is small, and therefore the value of slope is small. In water, because heat generated by cyclic deformation is transferred quickly to water and spread out, temperature of the specimen slightly increases. Therefore $N_f$ is large and slope is large in water.

### 3.3. Formulation of low-cycle fatigue life

**3.3.1. Dependence on strain amplitude.** As found from the strain-life curves shown in Fig. 1, the relationship between strain amplitude $\varepsilon_a$ and the number of cycles to failure $N_f$ in the region of low-cycle fatigue on a logarithmic graph is practically expressed by a straight line. Therefore, similarly as in the case of Manson-Coffin relationship for steel in low-cycle fatigue, the relationship between $\varepsilon_a$ and $N_f$ for TiNi SMA may be expressed as follows

$$\varepsilon_a \cdot N_f^{\beta} = \alpha, \tag{3.2}$$

where $\alpha$ and $\beta$ represent $\varepsilon_a$ in $N_f = 1$ and the slope of the $\log\varepsilon_a - \log N_f$ curve, respectively. The value of $\beta$ in water is about 0.5 at each temperature. The same value is obtained for steel.

**3.3.2. Dependence on temperature.** The dependence of the fatigue life on temperature will be discussed for fatigue tests performed in water, in which case temperature of the specimen increases little. The exponent $\beta$ in Eq. (3.2) is about 0.5 at each temperature. The value of $\alpha$ decreases with increasing temperature $T$. As expressed by Eq. (3.1), the MT stress increases in proportion to $T$. If the MT stress is high, fatigue damage is large and the fatigue life is short, resulting in small $\alpha$. Based on these considerations, if the relationship between $\alpha$ and $T$ is plotted on a semilogarithmic graph, it is found that the relationship is expressed by a straight line. Therefore it becomes as follows

$$\alpha = \alpha_s \cdot 10^{-a(T-M_s)}, \tag{3.3}$$

where $M_s$ is 253 K which was obtained by the DSC test. Based on the results of the fatigue test in water, the coefficients in Eq. (3.3) are determined as $\alpha_s = 8.56$ and $a = 0.012$ K$^{-1}$. Therefore, from Eq. (3.2), the relationship between $\varepsilon_a$ and $N_f$ is expressed by the following equation

$$\varepsilon_a \cdot N_f^{0.5} = 8.56 \times 10^{-0.012(T-M_s)}. \tag{3.4}$$

Thus the dependence of the fatigue life on $\varepsilon_a$ and $T$ is described by Eq. (3.4).

**3.3.3 Evaluation of low-cycle fatigue life.** The experimental results between $\varepsilon_a$ and $N_f$ obtained in water and the calculated results obtained by Eq. (3.4) are shown in Fig. 3. As seen in Fig. 3, the experimental results are well expressed by the calculated results. Therefore the proposed relationship is useful for evaluation of low-cycle fatigue life when we design SMA elements.

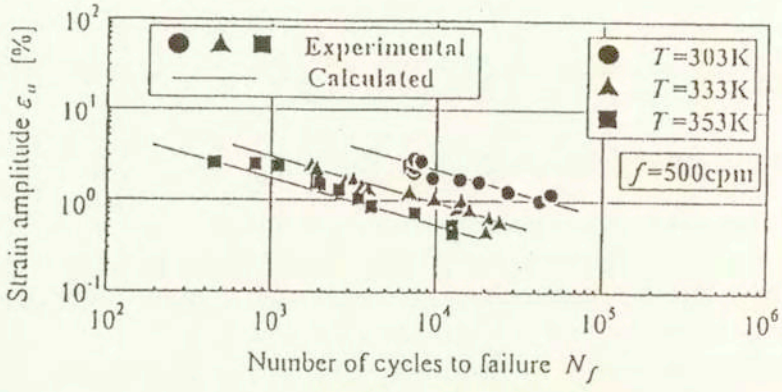


FIG. 3. Strain amplitude versus fatigue life for low-cycle fatigue region at various temperatures in water.

## 4. Heat engine

### 4.1. Tilt-disk offset SMA heat engine

The basic structure and working principle of a tilt-disk offset SMA heat engine are shown in Fig. 4.

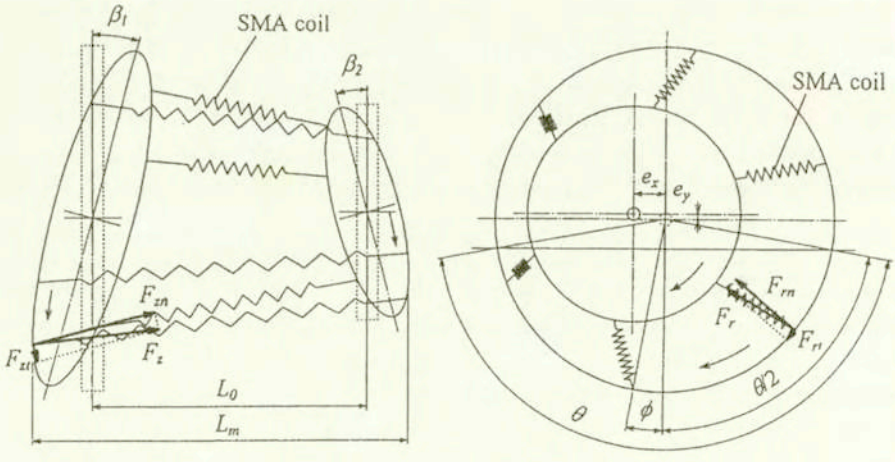


FIG. 4. Basic structure and working principle of a tilt-disk offset SMA heat engine.

The engine has two tilt disks which are facing each other. The axes of two disks are independent of each other. The center distance of two disks is $L_0$ in the horizontal direction. The two disks are eccentric by a distance of $e_x$ and $e_y$ in the horizontal and vertical directions, respectively. The disks are inclined by angles of $\beta_1$ and $\beta_2$ from the vertical direction, respectively. Each point on the circumferences of two disks is connected by a SMA helical spring. The circumference of a large disk corresponding to the heating angle $\theta$ is soaked in the hot reservoir. The center of the heating angle is inclined by the heating phase angle $\phi$ against the position where the SMA helical springs are most widely expanded. In the heating zone, the SMA coil contracts with radial component $F_r$ and axial component $F_z$ of the recovery force due to the reverse transformation. The tangential components $F_{rt}$ and $F_{zt}$ of the contraction force rotate the disks. The direction of rotation varies depending on $e_y$ and $\phi$.

#### 4.2 Output power

The tilt-disk offset SMA heat engine was constructed. The output power characteristics were examined. The experimental conditions were as follows. The heating zone was in hot water and the cooling zone in air. The number of SMA coils was 12, $e_x = 5$ mm, $e_y = 0$ mm, $\beta_1 = 15°$, $\beta_2 = 0°$, $\theta = 160°$, $\phi = 40°$ and $L_0 = 110$ mm.

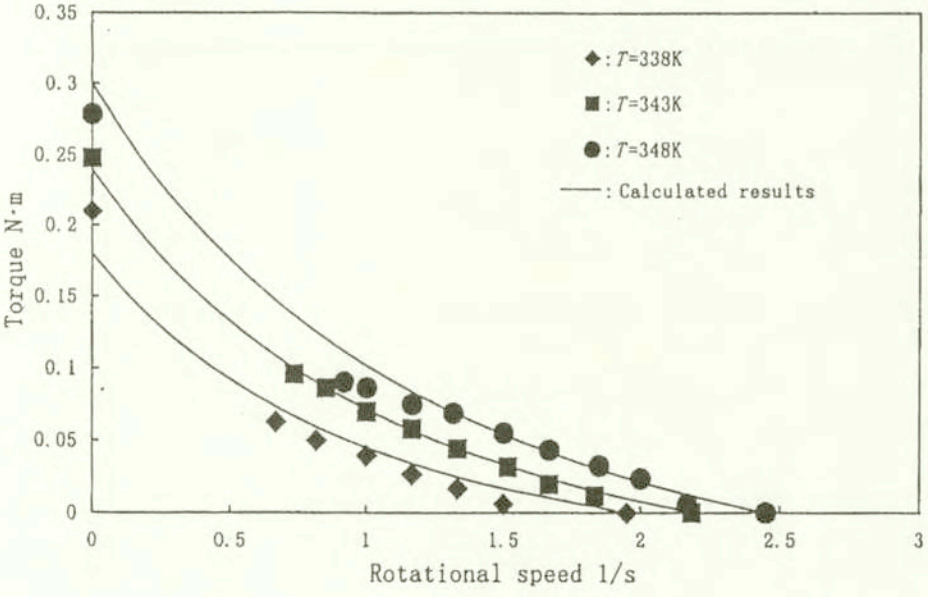


FIG. 5. Relationship between torque and rotational speed.

The relationship between torque $M$ and rotational speed $n$ obtained by the experiments at various temperatures $T$ is shown in Fig. 5. As seen in Fig. 5, the torque decreases with an increase in rotational speed. The relationship between $M$ and $n$ can be expressed by a simple power function as follows

$$(M + M_0)(n + n_0)^b = c, \tag{4.1}$$

where $n_0$ denotes rotational speed under no torque and $c = M_0(2n_0)^b$. Torque at $n = 0$ is $(2^b - 1)M_0$.

The recovery stress increases in the reverse transformation region and can be approximated by a linear relationship of temperature [14, 15]. Therefore stationary torque $M_0$ can be expressed as function of temperature as follows:

$$M_0 = h(T - A_f) + m. \tag{4.2}$$

On the other hand, $n_0$ depends not only on temperature but also on viscosity of water and friction among elements of the engine. Thus $n_0$ is expressed by the following equation:

$$n_0 = k(T - A_f) + \nu. \tag{4.3}$$

The dependence of $M_0$ and $n_0$ on $T$ is shown in Fig. 6. As seen in Fig. 6, the dependence of $M_0$ and $n_0$ on $T$ is well expressed by Eqs. (4.2) and (4.3), respectively.

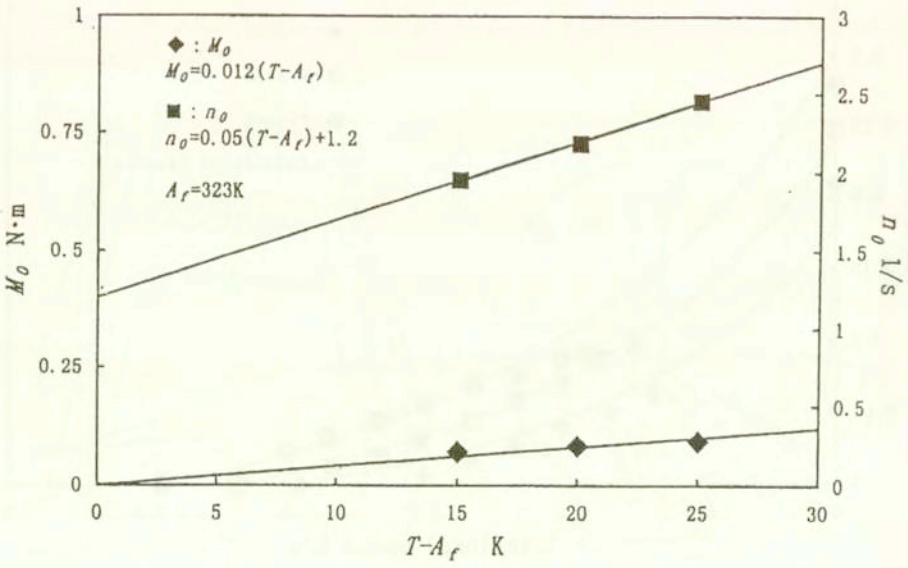


FIG. 6. $M_0$ and $n_0$ versus temperature.

Based on Eq. (4.1), the output power $P$ can be obtained as follows:

$$P = 2\pi nM = 2\pi M_0 n \times \left\{ \left( \frac{2n_0}{n+n_0} \right)^b - 1 \right\}. \tag{4.4}$$

The relationship between $P$ and $n$ at various $T$ is shown in Fig. 7. As seen in Fig. 7, the output characteristic are estimated by Eq. (4.4). Therefore Eq. (4.4) is used to obtain the optimum operating condition of SMA heat engines.

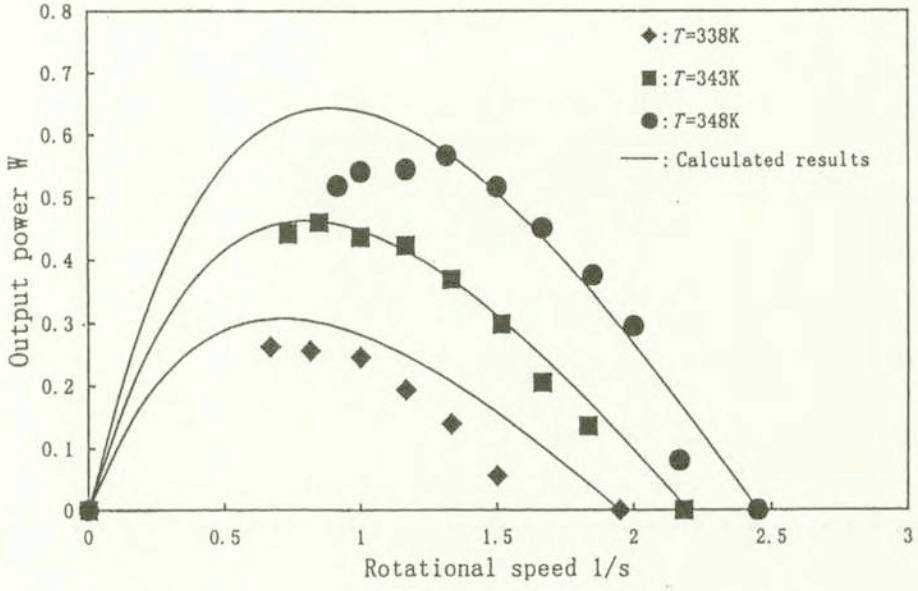


FIG. 7. Relationship between output power and rotational speed.

## 5. Thermal actuator

### 5.1. Indirect-heated SMA actuator

Thermal actuators heating with direct electric current have been investigated in various fields. Low-level electric current is required in the case of application for vehicles because of the limitation of electric source. The target of this research is focused on indirect heating of SMA using a fine wire with low level electric current. This section reports the recent activities on improving the response of an indirect-heated SMA actuator.

Enlarged view of section of a SMA wire wound by a fine wire is shown in Fig. 8(a). Air gap exists between a fine wire and a SMA wire, and thus it has

effect of decreasing heat conduction from a fine wire to a SMA wire. The material with high heat conduction coefficient is plastered between a fine wire and a SMA wire to improve heat conduction as shown in Fig. 8(b).

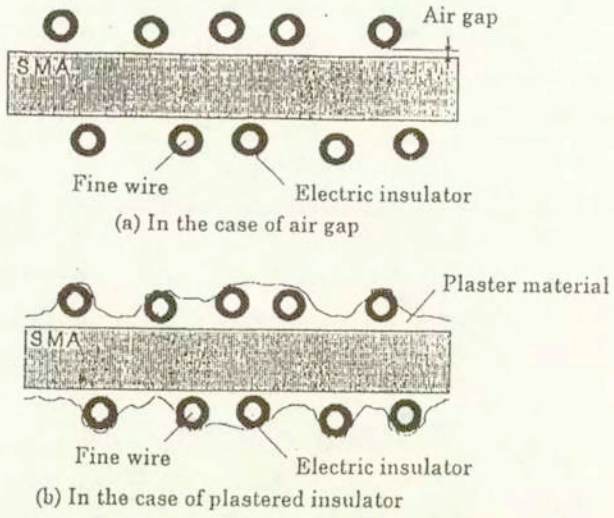


FIG. 8. Enlarged view of section.

Fig. 9 shows schematically the layout of elements in the indirectly heated SMA actuator.

Based on Fourier's law, transported heat $(dq)$ from a fine wire at $T_f$ to a SMA wire at $T$ in small period $(d\tau)$ is expressed as follows:

$$dq = \frac{2\pi(T_f - T)l}{\frac{1}{\lambda_2}\log\left(\frac{r_0 + b_2}{r_0}\right) + \frac{1}{\lambda_1}\log\left(\frac{r_0 + b_2 + b_1}{r_0 + b_2}\right)} d\tau, \tag{5.1}$$

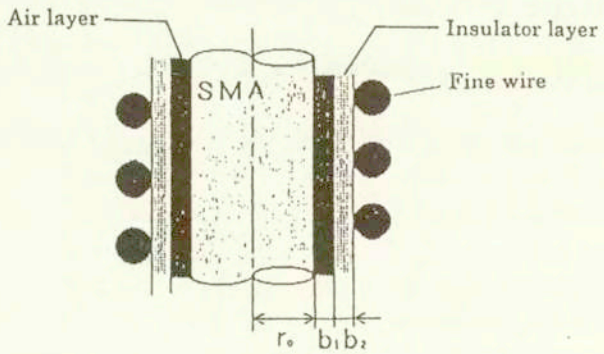


FIG. 9. Heat conduction model.

where $l$, $T$, $\tau$ and $\lambda$ denote length of SMA, temperature, time and thermal conductivity, respectively. Subscripts 1 and 2 denote air and insulator, respectively. The characteristic values $k_1$, $k_2$ and $k_3$ of size and materials are introduced as follows:

$$k_1 = r_0^2 \gamma_0 C_0, \quad k_2 = \frac{1}{\lambda_2} \log\left(\frac{r_0 + b_2}{r_0}\right), \quad k_3 = \frac{1}{\lambda_1} \log\left(\frac{r_0 + b_2 + b_1}{r_0 + b_2}\right), \tag{5.2}$$

where $\gamma_0$ and $C_0$ denote density and specific heat of SMA, respectively.
The overall index $K$ is obtained as follows:

$$K = \frac{1}{k_1(k_2 + k_3)}. \tag{5.3}$$

Non-dimensional temperature is defined by the following equation:

$$t = 1 - e^{-2K\tau}. \tag{5.4}$$

### 5.2. Time constant and working force

Many samples with various sizes and materials were presented in this research and response times were measured. The results are summarized in Fig. 10. As found from Fig. 10, the guideline to get high response of the SMA actuator is obtained. As found from Eqs. (5.2) and (5.3), if we use a SMA wire with diameter of a half, time constant decreases by about one fourth.

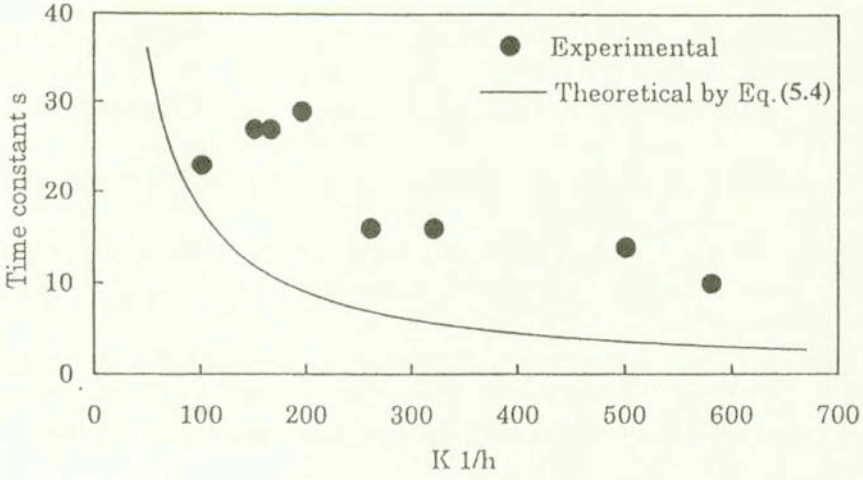


FIG. 10. Experimental and theoretical values of time constant.

Using the model which showed highest responsibility, a coiled spring actuator was manufactured. The measured response of force after electric current supply is shown in Fig. 11. The working force covers a target value. These investigations should contribute to the development of a new high-performance thermal actuator with indirect heating.

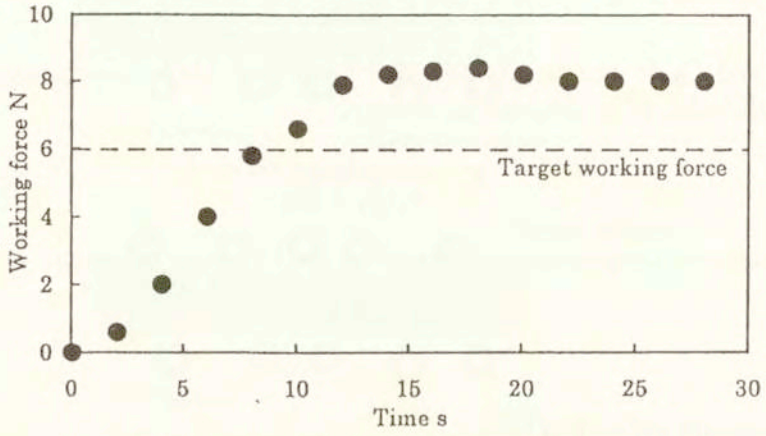


FIG. 11. Relationship between working force and time.

## 5. Conclusions

The fatigue properties of the TiNi SMA wire subjected to rotating bending have been investigated experimentally. A tilt-disk offset SMA heat engine and an indirect-heated SMA thermal actuator are developed. The main results obtained are summarized as follows.

1. If the strain amplitude is found in the RPT region, the fatigue life is longer than $10^7$ cycles. If the strain amplitude is found in the MT region, the fatigue life is shorter than $10^5$ cycles. The dependence of low-cycle fatigue life on temperature is expressed by the proposed fatigue equation.

2. The working properties of the tilt-disk SMA heat engine depend on various parameters.

The dependence of output power characteristics on temperature is estimated by the proposed equation. The optimum operating condition of the SMA heat engine is evaluated.

3. The heat conduction model of the indirect-heated SMA actuator is proposed. The time constant and working force are evaluated by the proposed model. The condition to develop the indirect-heated SMA actuator is clarified.

## Acknowledgements

The authors wish to express their gratitude to Polish Academy of Sciences, Japan Society for the Promotion of Science and the Nitto Foundations for financial supports.

## References

1. J. PERKINS [Ed.], *Shape memory effects in alloys*, Plenum Press, New York 1975.
2. H. FUNAKUBO [Ed.], *Shape memory alloys*, Gordon and Breach Science Pub., New York 1987.
3. K. OTSUKA, *Introduction to the R-phase transition*, 36–45 [in:] Engineering aspects of shape memory alloys, T. W. Duerig, K. N. Melton, D. Stockel, C. M. Wayman, [Eds.], Butterworth-Heinemann, London 1990.
4. S. MIYAZAKI and K. OTSUKA, *Deformation and transition behavior associated with the R-phase in Ti-Ni alloys*, Metall. Trans. A, **17A**, 53–63, 1986.
5. H. TOBUSHI, S. YAMADA, T. HACHISUKA, A. Ikai and K. TANAKA, *Thermomechanical properties due to martensitic and R-phase transformations of TiNi shape memory alloy subjected to cyclic loadings*, Smart Mater. Struct., **5**, 788–795, 1996.
6. H. TOBUSHI, T. HACHISUKA, T. HASHIMOTO and S. YAMADA, *Cyclic deformation and fatigue of a TiNi shape-memory alloy wire subjected to rotating bending*, Trans. ASME, J. Eng. Mater. Tech, **120**, 64–70, 1998.
7. K.N. MELTON and O. MERCIER, *Fatigue of NiTi thermoelastic martensites*, Acta Metall., **27**, 137–144, 1979.
8. S. MIYAZAKI, *Development and characterization of shape memory alloys*, 69–147 [in:] Shape memory alloy, M. Fremond and S. Miyazaki, Springer Wien, New York 1996.
9. W.S. GINELL, J.L. MCNICHOLS, Jr. and J.S. CORY, *Nitinol heat engines for low-grade thermal energy conversion*, Mech. Eng., **101**, 5, 28–33, 1979.
10. H. TOBUSHI, K. KIMURA, H. IWANAGA and J.R. CAHOON, *Basic research on shape memory alloy heat engine (Output power characteristics and problems in development)*, JSME Inter. J., Ser. I, **33**, 2, 263–268, 1990.
11. H. TOBUSHI, T. HACHISUKA. S. YAMADA and P.H. LIN, *rotating -bending fatigue of aTiNi shape-memory alloy wire*, Mech. Mater., **26**, 35–42, 1997.
12. K. TANAKA, S. KOBAYASHI and Y. SATO, *Thermomechanics of transformation pseudoelasticity and shape memory effect in alloys*, Inter. J. Plasticity, **2**, 59–72, 1986.
13. H. TOBUSHI, P.H. LIN, K.TANAKA, C. LEXCELLENT and A. IKAI, *Deformation properties of TiNi shape memory alloy*, J. de Phys. IV, C2, **5**, 409–413, 1995.
14. K. TANAKA, T. HAYASHI, Y. ITOH and H. TOBUSHI, *Analysis thermomechanical behavior of shape memory alloys*, Mech. Mater., **13**, 207–215, 1992.
15. P.H. LIN, H. TOBUSHI, K. TANAKA, C. LEXCELLENT and A. IKAI, *Recovery Stress of TiNi shape memory alloy under constant strain*, Arch. Mech., **47**, 2, 281–293, 1995.

*Received January 13, 1999; new version April 19, 1999.*